Semiclassical molecular dynamics simulations of excited state double-proton transfer in 7-azaindole dimers

Victor Guallar, Victor S. Batista, and William H. Miller[a)]
Department of Chemistry, University of California, and Chemical Sciences Division, Lawrence Berkeley National Laboratory, Berkeley, California 94720

(Received 14 January 1999; accepted 3 March 1999)

An *ab initio* excited state potential energy surface is constructed for describing excited state double proton transfer in the tautomerization reaction of photo-excited 7-azaindole dimers, and the ultrafast dynamics is simulated using the semiclassical (SC) initial value representation (IVR). The potential energy surface, determined in a reduced dimensionality, is obtained at the CIS level of quantum chemistry, and an approximate version of the SC-IVR approach is introduced which scales *linearly* with the number of degrees of freedom of the molecular system. The accuracy of this approximate SC-IVR approach is verified by comparing our semiclassical results with full quantum mechanical calculations. We find that proton transfer usually occurs during the first intermonomer symmetric-stretch vibration, about 100 fs after photoexcitation of the system, and produces an initial 15 percent population decay of the reactant base-pair, which is significantly reduced by isotopic substitution. [S0021-9606(99)01820-6]

I. INTRODUCTION

Proton transfer in hydrogen-bonded complexes is one of the most fundamental chemical reactions and has therefore been extensively investigated,[1–10] not only because it involves a quantum mechanical process that is yet to be fully understood, but also because it is a ubiquitous phenomenon which influences the dynamical behavior of a wide variety of systems. In particular, the mechanisms of excited state double-proton transfer after photoexcitation of canonical base pairs have attracted a great deal of experimental and theoretical interest[11–37] because of its implication in radiation-induced mutations or carcinogenesis resulting from the possible existence of the rare enol tautomeric forms of the bases during DNA replication.[38–41]

However, a detailed understanding of the dynamical processes involved in these tautomerization reactions is still a goal of current investigations.[32–35] Computational methods able to provide a microscopic description of the involved proton transfer dynamics are the subject of much current theoretical research.[42–57] However, applications to these excited state tautomerization reactions are yet to be carried out, since these relatively large molecular systems present the challenge of modeling multiple time scale dynamics with significant motion of light atoms, where the quantum phenomenon of proton tunneling can be significant at low temperatures and determine the rate of the overall chemical reaction. In this paper we report the first application of molecular dynamics simulation methods to model the excited state double-proton transfer dynamics involved in the tautomerization reaction of the 7-azaindole dimers. Simulations are based on an approximate version of the semiclassical (SC) initial value representation (IVR) utilizing a 3-dimensional excited state potential energy surface (PES) constructed at the *ab-initio* quantum chemistry CIS level of theory.

The 7-azaindole dimer is often considered to be a paradigm system for photo-induced double-proton transfer in DNA base-pairs and has been the subject of experimental studies in solution, matrices, and supersonic-jet expansions which have provided indirect photochemical information of the double-proton transfer mechanism.[13–18] This early experimental work followed the initial discovery that certain conformational isomers could undergo cooperative double-proton transfer upon ultraviolet irradiation, as manifested by the large Stokes shift of the fluorescence spectra with dual bands in the uv-vis region.[13] The structural diagram describing the excited state double-proton transfer in 7-azaindole dimers is as follows:

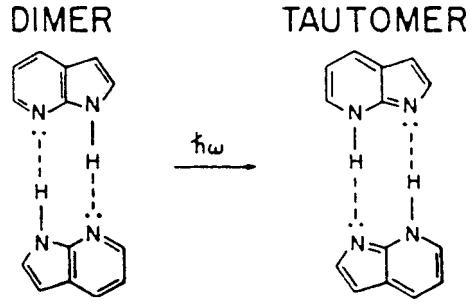

(scheme)

where $\hbar\omega$ is the excitation energy. In an effort to elucidate the reaction mechanism, a variety of ultrafast spectroscopic studies have been recently performed probing both the tautomeric and dimeric excited state relaxation processes with

a)Electronic mail: miller@neon.cchem.berkeley.edu

picosecond and subpicosecond resolution.[29–37] Various possible interpretations have been suggested on the basis of the analysis of the experimental signals, including the possibility of a step-wise reaction mechanism involving a zwitterionic intermediate,[31] or ultrafast interconversion to some intermediate electronic state before undergoing double-proton transfer reaction.[32,33] In particular, the interpretation of experimental spectra showing evidence for the quantum phenomenon of proton tunneling as the dominant mechanism for tautomerization at low temperatures was, in general, based on a one- dimensional double minimum potential model[39] with an estimated barrier height of 1.2–1.4 kcal/mol describing the energetics of the reaction.[16,29,31] Ideally, however, one would like to provide a more rigorous interpretation of the experiments based on a quantitative description of reaction dynamics from first principles, since fitting the experimental values of rate constants using a one-dimensional model may not necessarily yield a potential that bears any simple relation to the true Born–Oppenheimer potential energy surface describing this particular double-proton transfer reaction. The reason for this is that the rate of double-proton transfer in the photo-excited 7-azaindole dimers is significantly enhanced by excitation of vibrational modes.[18,31] It is therefore essential to combine experimental studies with more realistic theoretical simulations to develop an understanding of the underlying proton transfer dynamics as coupled to the other degrees of freedom in the system.[43,58] This could be accomplished by first calculating the full *ab-initio* Born–Oppenheimer potential energy surfaces and then solving accurately the dynamical equations for motion on these calculated surfaces.

In an effort to investigate the potential energy surfaces involved in the double-proton transfer mechanism, semi-empirical[23–26] and *ab-initio* quantum chemistry CIS calculations[21] have been performed for describing the fully optimized geometries of the base-pair, intermediate, tautomer and transition states of the 7-azaindole dimer. However, the possibility of mapping out the entire potential energy surface in its full dimensional configuration space is daunting because of the enormous number of calculations required by the high dimensionality of the potential energy surface. A variety of methods have been suggested for making the best use of a reasonable number of potential energy calculations for purposes of studying molecular dynamics of polyatomic molecular systems, including the reaction path method, where one computes the potential energy surface only for a one-dimensional curve in the multidimensional space that connects the reactants and product configurations.[59–65] However, most of these methods are not adequate for modeling double-proton transfer dynamics in 7-azaindole dimers because the tautomerization reaction involves significant tunneling motion of light atoms, which is not confined to small amplitude fluctuations around a reaction path and is coupled to the motion of other degrees of freedom in the system. In this paper we develop a 3-dimensional excited state potential energy surface in terms of a reaction surface model obtained at the *ab-initio* CIS level of theory, where the proton displacement r_1 and the intermonomer symmetric-stretch modes r_2 are described as large amplitude coordinates.[43,66–71] The reaction surface is obtained by minimizing the excited state potential energy of the molecular system through geometry optimization with respect to the remaining (weakly coupled) degrees of freedom $\mathbf{z}$, subject to the constraints of fixed values for r_1 and r_2 at various base-pair, intermediate, tautomer and transition state configurations. The global potential energy surface is obtained expanding the $\mathbf{z}$ dependence to second order about the equilibrium coordinates $\mathbf{z_0(r_1,r_2)}$, and its dimensionality is reduced from N to 3 defining a global reorganization coordinate to describe, on average, the motion of the $(N-2)$ locally harmonic degrees of freedom $\mathbf{z}$.

Simulating the excited state dynamics of proton transfer is particularly challenging because the protons being transferred give rise to significant quantum mechanical effects —i.e., tunneling— which cannot be described by classical molecular dynamics simulations. A number of mixed quantum-classical molecular dynamics methods have been applied to simulations of proton transfer reactions.[72–83,53] Most of these methods, however, describe only approximately the coupling between light and heavy particle degrees of freedom according to branching processes defined by stochastic hops that collapse transferring protons into either of the possible states of distinct character. Other methods are applicable only to single-proton transfer reactions, or model light and heavy degrees of freedom on different dynamical footing. In this paper we present the implementation of an approximate version of the SC-IVR approach, which models the motion of light and heavy degrees of freedom on the same dynamical footing and also properly describes the multidimensional mechanism of proton tunneling as determined by the coupling of proton motion to the remaining degrees of freedom in the system.

The approximation we introduce to the SC-IVR approach has to do with the calculation of the monodromy matrix elements that are involved in the pre-exponential factor of the semiclassical amplitude (*vide infra*). Their calculation, in general, requires the integration of N^2 equations (where N is the number of degrees of freedom) and is therefore the bottleneck for the application of the SC-IVR approach to large molecular systems. The approximation described in Sec. II A (and in the Appendix) reduces this to the integration of only N equations, thus scaling with molecular size in the same way as the classical trajectory equations themselves. Our aim in this first application study is to explore the capabilities of this approximate version of the SC-IVR through direct comparison with full quantum mechanical calculations. At this point we do not attempt to reproduce the results of specific experiments but rather to provide a rigorous description of dynamics on well-characterized electronic state potential energy surfaces.

The paper is organized as follows: In Sec. II A we first outline the semiclassical approach for calculating the time dependent reactant survival probability, according to the approximate SC-IVR method described in the Appendix. In Sec. II B we characterize the nature of the $S1$ electronic excited state of the 7-azaindole dimer $(7AI)_2$, and present the comparison with the corresponding low-lying excited state of the monomer $7AI$. In Sec. II C we describe the cal-

culation of the *ab-initio* $S1$ reaction surface potential in an expanded low dimensionality space. In Sec. III we present our results and compare them with full quantum calculations. The analysis of the double-proton transfer dynamics is concluded in Sec. IV, where the reaction mechanism suggested by our SC MD simulation results is compared to the reaction mechanisms postulated by recent ultrafast spectroscopic studies.

II. METHODS

A. The semiclassical approach

The quantity of interest is the reactant survival probability $P(t)$, defined as the probability that at time t the system is still on the reactant side of the dividing surface (in coordinate space) that separates reactants and products,

$$P(t)\equiv\langle\Psi_0|e^{i\hat{H}t/\hbar}h(\mathbf{q})e^{-i\hat{H}t/\hbar}|\Psi_0\rangle. \tag{2.1}$$

Here $\hat{H}$ is the Hamiltonian operator of the molecular system, $\mathbf{q}$ represents the mass-weighted nuclear internal coordinates of the molecular system, and $h(\mathbf{q})$ is a function of the proton coordinates that is 1(0) on the reactant (product) side of the dividing surface. The initial state on the S_1 PES is assumed to be the ground vibrational state of S_0,

$$\langle\mathbf{q}|\Psi_0\rangle=\prod_{j=1}^{N}\left(\frac{\alpha_j}{\pi}\right)^{1/4}\exp\left(-\frac{\alpha_j}{2}q(j)^2\right), \tag{2.2}$$

where $q(j)$ is the j-th coordinate; $\alpha_j=\sqrt{k_j\mu_j/\hbar^2}$, where k_j is the j-th harmonic constant, and μ_j represents the j-th reduced mass. The initial wavefunction, Eq. (2.2), is constructed on the basis of the low temperature approximation —i.e., assuming that contributions from anharmonicity and higher vibrational levels can be neglected— since measured experimental tautomerization rates were found to vary only slightly at temperatures lower than 77 K.[15]

The Herman–Kluk (HK),[49] or coherent state IVR for the time evolution operator, is

$$e^{-(\frac{i}{\hbar})\hat{H}t}=(2\pi\hbar)^{-N}\int d\mathbf{p_0}\int d\mathbf{q_0}e^{iS_t(\mathbf{p_0},\mathbf{q_0})/\hbar}C_t(\mathbf{p_0},\mathbf{q_0})\times|g_{\mathbf{q}_t,\mathbf{p}_t}\rangle\langle g_{\mathbf{q_0},\mathbf{p_0}}|, \tag{2.3}$$

where the wavefunction for the coherent states is

$$\langle\mathbf{q}|g_{\mathbf{q}_0,\mathbf{p}_0}\rangle=\prod_{j=1}^{N}\left(\frac{2\gamma(j)}{\pi}\right)^{1/4}\exp\left(-\gamma(j)[q(j)-q_0(j)]^2+\frac{i}{\hbar}p_0(j)[q(j)-q_0(j)]\right), \tag{2.4}$$

and similarly for $\langle\mathbf{q}|g_{\mathbf{q}_t,\mathbf{p}_t}\rangle$.

The integration variables $(\mathbf{p_0},\mathbf{q_0})$ in Eq. (2.3) are the initial conditions for classical trajectories, and $\mathbf{q}_t\equiv\mathbf{q}_t(\mathbf{p_0},\mathbf{q_0})$ and $\mathbf{p}_t\equiv\mathbf{p}_t(\mathbf{p_0},\mathbf{q_0})$ are the time-evolved coordinates and momenta. $S_t(\mathbf{p_0},\mathbf{q_0})$ is the classical action along this trajectory, obtained by integrating the following equation:

$$\dot{S}_t=\mathbf{p}_t\cdot\dot{\mathbf{q}}_t-H(\mathbf{p}_t,\mathbf{q}_t), \tag{2.5}$$

along with the usual classical equations of motion, and the pre-exponential factor $C_t(\mathbf{p_0},\mathbf{q_0})$ involves the monodromy matrix (see the Appendix).

The survival probability is thus given by

$$P(t)=(2\pi\hbar)^{-2N}\int d\mathbf{p_0}\int d\mathbf{q_0}\int d\mathbf{p'}_0\int d\mathbf{q'}_0\times e^{i(S_t(\mathbf{p_0},\mathbf{q_0})-S_t(\mathbf{p'}_0,\mathbf{q'}_0))/\hbar}\times C_t(\mathbf{p_0},\mathbf{q_0})C_t^*(\mathbf{p'}_0,\mathbf{q'}_0)\langle\Psi_0|\mathbf{p'}_0,\mathbf{q'}_0\rangle\times\langle\mathbf{p'}_t,\mathbf{q'}_t|h|\mathbf{p}_t,\mathbf{q}_t\rangle\langle\mathbf{p}_0,\mathbf{q}_0|\Psi_0\rangle. \tag{2.6}$$

Finally, in the Appendix we describe an approximation that we have used for the pre-exponential factor C_t, one that scales *linearly* with the number of degrees of freedom of the system. It is essentially an adiabatic approximation for the monodromy matrix elements and is given by

$$C_t(\mathbf{p_0},\mathbf{q_0})=\left[\prod_{j=1}^{N}\tilde{M}_t(j,j)\right]^{1/2}, \tag{2.7}$$

where $\tilde{M}_t(j,j)$ is defined as

$$\tilde{M}_t(j,j)=\frac{1}{2}\left(\tilde{Q}_t(j,j)+i\frac{\tilde{P}_t(j,j)}{\hbar 2\gamma(j)}\right), \tag{2.8}$$

where $\gamma(j)$ are the constant parameters in the coherent states of Eq. (2.4). The canonical variables $\tilde{Q}_t(j,j)$ and $\tilde{P}_t(j,j)$ are obtained by numerical integration of the following equations:

$$\dot{\tilde{Q}}_t(j,j)=\tilde{P}_t(j,j),\qquad\dot{\tilde{P}}_t(j,j)=\omega_t(j)^2\tilde{Q}_t(j,j), \tag{2.9}$$

with initial conditions $\tilde{Q}_0(j,j)=1$, and $\tilde{P}_0(j,j)=-i\hbar 2\gamma(j)$, where the instantaneous normal mode frequencies $\omega_t(j)$ are obtained by diagonalization of the Hessian along the classical trajectories.

As presented above, the computational task necessary to calculate the pre-exponential factor $C_t(\mathbf{p_0},\mathbf{q_0})$ is to integrate the N *independent* second-order differential equations introduced by Eq. (2.9). This constitutes a minor computational task when compared to the numerical effort involved in the diagonalization of the Hessian, and we thus solve it exactly according to the standard fourth-order Runge–Kutta method.[84] In the Appendix we also describe an approximate analytic solution that may be accurate and more efficient for applications with many locally harmonic degrees of freedom.

B. Molecular orbitals

In this section we characterize the $S1$ and $S2$ electronic excited states of the base pair 7-azaindole dimer $(7AI)_2$ in terms of the CIS eigenvectors, the optimized excited state energies, and the oscillator strength constants. We also compare these two states with the $S_1(\pi,\pi^*)$ and $S_2(\pi,\pi^*)$

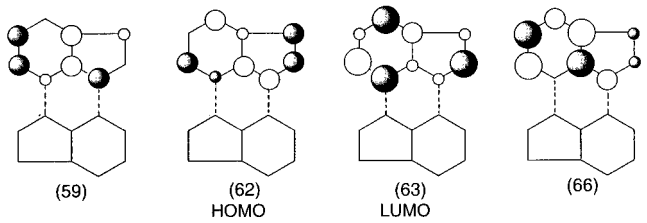

FIG. 1. Highest filled and lowest empty π molecular orbitals of 7-azaindole dimer calculated from CIS/6-31G for the S_1 optimized geometry structure. The circle diameters are proportional to the maximum p_z AO coefficients (no circle indicates a maximum coefficient smaller than 0.1; a small circle indicates maximum coefficients between 0.1 and 0.15, medium circle corresponds to coefficients between 0.15 and 0.3 and large circles indicate coefficients larger than 0.3; black and white indicate positive or negative sign).

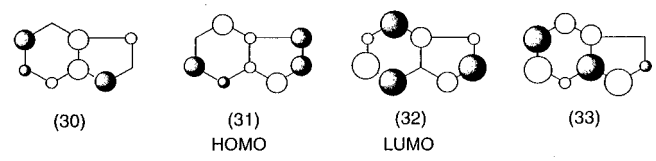

FIG. 2. Highest filled and lowest empty π molecular orbitals of 7-azaindole monomer calculated from CIS/6-31G for the S_1 optimized geometry structure. The circle diameters are proportional to the maximum p_z AO coefficients (no circle indicates a maximum coefficient smaller than 0.1, a small circle indicates maximum coefficients between 0.1 and 0.15, a medium circle corresponds to coefficients between 0.15 and 0.3 and large circles indicate coefficients larger than 0.3; black and white indicate a positive or negative sign).

electronic excited states of the 7-azaindole monomer $7AI$, which are found to be analogous to the ^1L_a and ^1L_b states, respectively, of linear condensed-ring molecules.[85,86]

Figure 1 shows the π MOs (59), (62), (63) and (66) of the $(7AI)_2$ base-pair at the $S1$ minimum energy geometry, in terms of the maximum p_z atomic orbital (AO) coefficients represented in diagram form, where the distribution of nodes is given by the signs and relative values of the expansion coefficients. These MOs are responsible for the more important single excitations which determine the $S1$ and $S2$ electronic structures, as indicated by the CIS eigenvectors presented in Table I: the $S1$ state with a predominant contribution from the $(62)\rightarrow(63)$ MO excitation, and the $S2$ state with an admixture of the $(59)\rightarrow(63)$ and the $(62)\rightarrow(66)$ MO excitations. Figure 1 shows that the four molecular orbitals are localized in the upper monomer, representing the monomer that undergoes preferential rearrangements when the geometry of the base-pair is optimized according to the $S1$ or $S2$ electronic excited state PESs. Under such a geometry optimization process, the other moiety preserves approximately its ground electronic state minimum energy geometry and localizes the π MOs (60), (61), (64) and (65)—not displayed in Fig. 1—which are analogous to the π MOs (59), (62), (63) and (66), respectively.

Figure 2 shows the key π MOs of the 7-azaindole monomer —i.e., the (HOMO-1), HOMO, LUMO and (LUMO +1)— which according to the CIS eigenvectors presented in Table I are responsible for the single excitations that determine the $S1$ and $S2$ electronic structures of the monomer $7AI$. The S_1 excited state involves primarily the (HOMO) $\rightarrow$ (LUMO) excitation, and an important amount of (HOMO-1) $\rightarrow$ (LUMO+1). The S_2 state is a mixture of (HOMO) $\rightarrow$ (LUMO+1), and (HOMO-1) $\rightarrow$ (LUMO) MO excitations.

The comparison of the molecular orbitals indicates that the MOs (59), (62), (63) and (66) are approximately the (HOMO-1), (HOMO), (LUMO) and (LUMO+1) of the moiety that undergoes reorganization, while the MOs (60), (61), (64) and (65) are the analogous MOs of the monomer that preserves approximately its ground state geometry. The CIS/6-31G eigenvectors, optimized energies and oscillator strength constants presented in Table I indicate that although the $S1$ and $S2$ excited states are somewhat affected by dimerization they still preserve their own electronic nature. The electronic excited state analogous to the ^1L_a state of condensed ring molecules—i.e., the S_1 state— is lower in energy, and has a larger oscillator strength constant than the electronic state analogous to ^1L_b state of condensed ring molecules —i.e., the S_2 state— and this holds for both the $7AI$ monomer and the $(7AI)_2$ base-pair molecular systems.

C. Excited state potential energy surface

In this section we develop a 3-dimensional potential energy surface to describe the excited state double-proton transfer in 7-azaindole dimers. The model is based on CIS reaction surface potentials $V_0^{(\zeta)}(r_1,r_2)$ for the two low-lying singlet electronic excited states that define the S_1 PES, for the r_1 and r_2 range of configurations explored in our simulation study. $V_0^{(\zeta)}(r_1,r_2)$ are thus parametrized by the one-dimensional proton coordinate r_1, and the intermonomer

TABLE I. CIS eigenvectors, optimized energies and oscillator strength constants for the optimized S_1 and S_2 electronic excited states of the 7-azaindole dimer $(7AI)_2$ and 7-azaindole monomer $7AI$.

Electronic state	$S_1(\pi,\pi^*),(7AI)_2$	$S_2(\pi,\pi^*),(7AI)_2$	$S_1(\pi,\pi^*),7AI$	$S_2(\pi,\pi^*),7AI$
Optimized energy	5.07 eV	5.70 eV	5.28 eV	5.83 eV
Oscillator strength	f=0.33	f=0.09	f=0.38	f=0.07
CIS excitation	(62)→(63)	(62)→(66)	(31)→(32)	(31)→(33)
CIS coefficient	0.66	−0.27	0.66	−0.28
CIS excitation	(59)→(66)	(59)→(63)	(30)→(33)	(30)→(32)
CIS coefficient	0.17	0.57	0.18	0.55

symmetric-stretch coordinate r_2; r_1 describes the sequential proton displacements in a nonconcerted double-proton transfer mechanism, and r_2 determines the intermonomer separation.

The CIS calculations of the reaction surface potentials $V_0^{(\zeta)}(r_1,r_2)$ show that concerted proton displacements involve higher energy configurations, and that for most of the nuclear configurations the first singlet electronic excited state $S1$ corresponds to the eigenstate with a predominant contribution from the (62)→(63) MO single excitation. Such an excited electronic state has an intermediate with zwitterionic character, that we denote here as INT.(Z), and results from the partial charge separation associated with the first proton transfer from the moiety that localizes the electronic excitation to the other. However, there are some molecular configurations around the minimum energy geometry of the INT.(Z) where another eigenstate becomes the lowest singlet excited state. Such an eigenstate has a predominant contribution from the (62)→(64) MO single excitation —i.e., involves an intermonomer electron transfer excitation from the MO (62), which is localized in the monomer that donates the first proton, to the MO (64) localized in the monomer where the first proton is transferred. The intermediate complex in that other electronic excited state thus involve a ''covalent'' electronic structure, since the charge associated with the first proton transferred is neutralized by the intermonomer electron transfer excitation, and is denoted here as INT.(C).

The Born–Oppenheimer PES that describes the $S1$ electronic excited state of the molecular system is obtained from the quantum chemistry calculation with the two-state wave function,

$$|\Psi\rangle = a_z|\psi_z\rangle + a_c|\psi_c\rangle, \tag{2.10}$$

where $|\psi_z\rangle$ describes the ''zwitterionic'' electronic state, and $|\psi_c\rangle$ is the ''covalent'' state wavefunction. The lowest electronic eigenvalue, i.e., the Born–Oppenheimer PES, $V_{B.O.}(\mathbf{q})$, is then given by the root of the 2×2 secular equation written in terms of the ''zwitterionic'' and ''covalent'' PESs, $V^{(z)}$ and $V^{(c)}$, and the exchange (or resonant) matrix elements which are approximated as constants ($\sim$1.5 kcal/mol) to match the energy gap at the crossings between the two PESs. $V_{B.O.}(\mathbf{q})$ is thus developed in the spirit of the so-called empirical valence bond (EVB) method,[87,88] but contrary to the *empirical* valence bond method where no electronic matrix elements are actually calculated, we compute the two PESs $V^{(z)}$ and $V^{(c)}$ according to the reaction surface model in an expanded 3-dimensional space.[43]

The reaction surfaces $V_0^{(\zeta)}(r_1,r_2)$ are calculated at the *ab-initio* CIS/6-31G level of theory —i.e., all single excitation with a spin-restricted Hartree–Fock reference ground state (CIS), using the 6-31G basis set within the Gaussian 94 series of programs[89]— minimizing the potential energy of the molecular system in the electronic excited state ζ with respect to the remaining $(N\text{-}2)$ degrees of freedom $\mathbf{z}$, subject to the constraint of fixed values for r_1 and r_2 at selected configurations for the base-pair, intermediate, tautomer and transition states. The potential energy surfaces $V^{(\zeta)}$ are then obtained in terms of the reaction surfaces $V_0^{(\zeta)}(r_1,r_2)$, expanding the $\mathbf{z}$ dependence to second order about the equilibrium coordinates $\mathbf{z_0}(r_1,r_2)$,

$$V^{(\zeta)}(r_1,r_2,\mathbf{z}) = V_0^{(\zeta)}(r_1,r_2) + \frac{1}{2}[\mathbf{z}-\mathbf{z_0^{(\zeta)}}(r_1,r_2)] \cdot \mathbf{F}^{(\zeta)}(r_1,r_2)\cdot[\mathbf{z}-\mathbf{z_0^{(\zeta)}}(r_1,r_2)], \tag{2.11}$$

where $\zeta\equiv(Z,C)$ indicates the nature of the electronic excited state, and

$$F_{i,j}^{(\zeta)}(r_1,r_2) = \left(\frac{\partial^2 V^{(\zeta)}(r_1,r_2,\mathbf{z})}{\partial z_i\ \partial z_j}\right)_{\mathbf{z}=\mathbf{z}_0^{(\zeta)}(r_1,r_2)}. \tag{2.12}$$

We reduce the dimensionality of the system from N to 3, introducing a global reorganization coordinate $R\equiv|\mathbf{z}|$ —i.e., the norm of the (N-2) dimensional vector $\mathbf{z}$— to describe on average the motion of the locally harmonic degrees of freedom $\mathbf{z}$. In the reduced 3-dimensional space the potential energy surfaces introduced by Eq. (2.11) become

$$V^{(\zeta)}(r_1,r_2,R) \approx V_0^{(\zeta)}(r_1,r_2) + \frac{1}{2}[\omega_R^{(\zeta)}(r_1,r_2)]^2 \times [R-R_0^{(\zeta)}(r_1,r_2)]^2, \tag{2.13}$$

where $R_0^{(\zeta)}(r_1,r_2)$ is the norm of $\mathbf{z_0^{(\zeta)}}(r_1,r_2)$, and the average frequencies $\omega_R^{(\zeta)}(r_1,r_2)$ are computed according to

$$\omega_R^{(\zeta)}(r_1,r_2) \equiv \left(\frac{2[V^{(\zeta)}(r_1,r_2,R_0^{(\zeta)}(r_1(0),r_2(0))) - V_0^{(\zeta)}(r_1,r_2)]}{[R_0^{(\zeta)}(r_1(0),r_2(0)) - R_0^{(\zeta)}(r_1,r_2)]^2}\right)^{1/2}, \tag{2.14}$$

in terms of the reference geometry $(r_1(0),r_2(0))$ chosen to be the initial $r_1(0)$ equilibrium geometry of the base-pair at the fixed intermonomer separation defined by $r_2(0)$.

Figure 3 shows the CIS/6-31G energy data points $V_{opt}^{(\zeta)}(r_1(k),r_2)$, and the corresponding interpolation curves as a function of r_2 for the base-pair (B.P., $k=1$), transition state 1 [T.S.(1), $k=2$], intermediate [INT.= INT.(Z,C), $k=3$], transition state 2 (T.S.(2), $k=4$) and tautomer (TAU., $k=5$) at the optimized $r_1(k)$ configurations displayed in Fig. 4. The stationary state energies $V_{opt}^{(Z)}(r_1(k),r_2)$ define the reaction surface $V_0^{(Z)}(r_1,r_2)$ in terms of the Lagrange form of the interpolation polynomial,[90] where the proper asymptotic limits along the r_1 coordinate are enforced according to the CIS proton frequencies at the B.P. and TAU. equilibrium geometries $(r_1(1),r_2)$ and $(r_1(5),r_2)$, respectively. Figure 5 shows the reaction surface $V_0^{(Z)}(r_1,r_2)$ with three well defined local minima that correspond to the B.P., INT.(Z) and TAU. minimum energy geometries. The energies and r_2 coordinates of the three local minima are also displayed in Fig. 3, where it is shown that the TAU. minimum energy is $\sim$1.6 kcal/mol lower than the B.P. minimum energy geometry. Thus, our model describes the tautomerization reaction to be exothermic. The other important topological aspect shown in

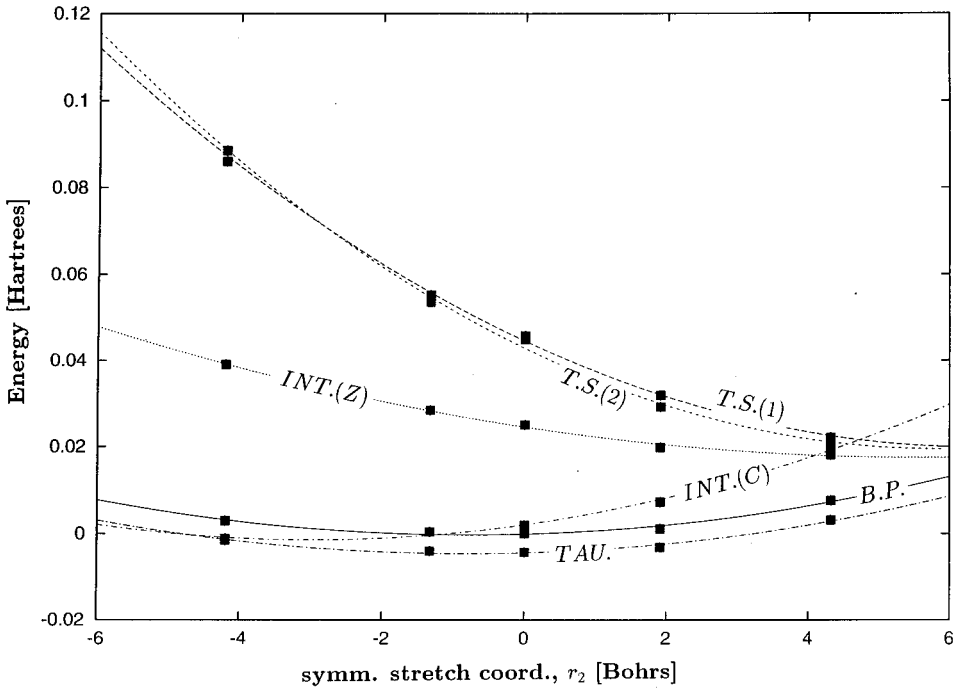

FIG. 3. CIS stationary state energies (solid squares) at various different intermonomer symmetric-stretch coordinate r_2 values in the -4.20–4.32 a.u. range, and interpolation curves.

Fig. 3 is the variation of the energy barrier between the B.P. and the zwitterionic intermediate—i.e., the T.S.(1) energy—as a function of r_2. The minimum energy barriers correspond to small intermonomer separations, in the $r_2 = 4$—6 a.u. range, where according to Fig. 4 the geometries of the base pair and intermediate states are closer together along the r_1 coordinate.

Figure 7 shows the average frequency $\omega_R^{(Z)}$ as a function of r_1 and r_2. According to the analysis of vibrational modes, the $\sim 900\ \mathrm{cm}^{-1}$ values in the B.P. region —i.e., $r_1 < s(r_2)$— have predominant contributions from the $C-C$, $C-N$ and intermonomer asymmetric stretching modes, while the low frequency values in the intermediate region between the two transition states have predominant contributions from the intermonomer bending modes ($\sim 350\ \mathrm{cm}^{-1}$).

Figure 8 shows $R_0^{(z)}$ as a function of the reaction surface coordinates r_1 and r_2. This figure shows that according to our model potential the maximum reorganization relative to

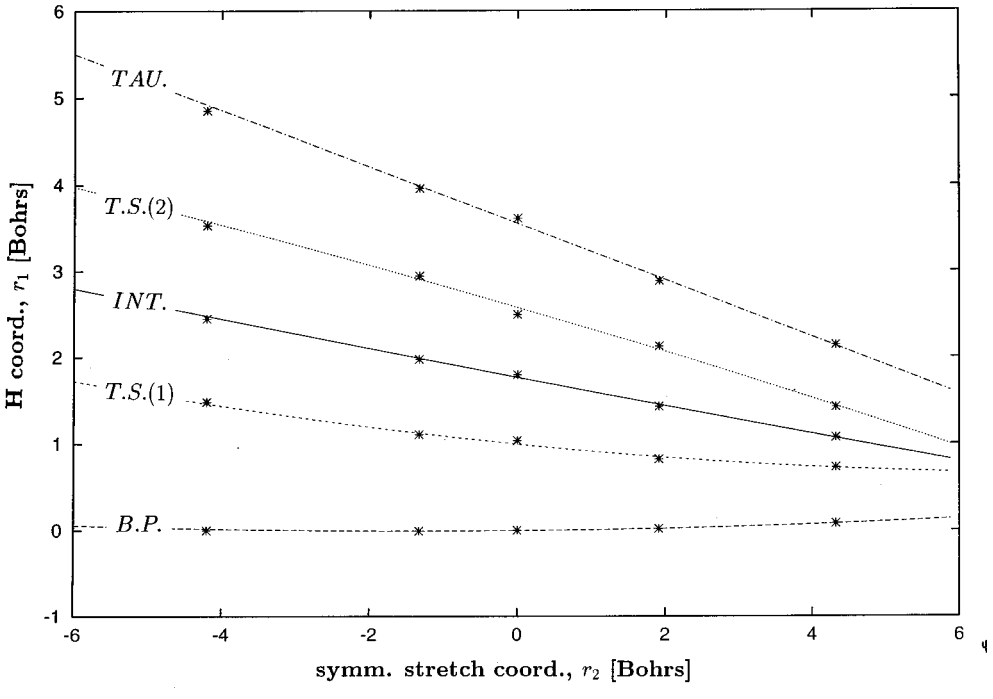

FIG. 4. CIS equilibrium geometries r_1 (stars) at various different intermonomer symmetric-stretch coordinate r_2 values in the -4.20–4.32 a.u. range, and the corresponding interpolation curves.

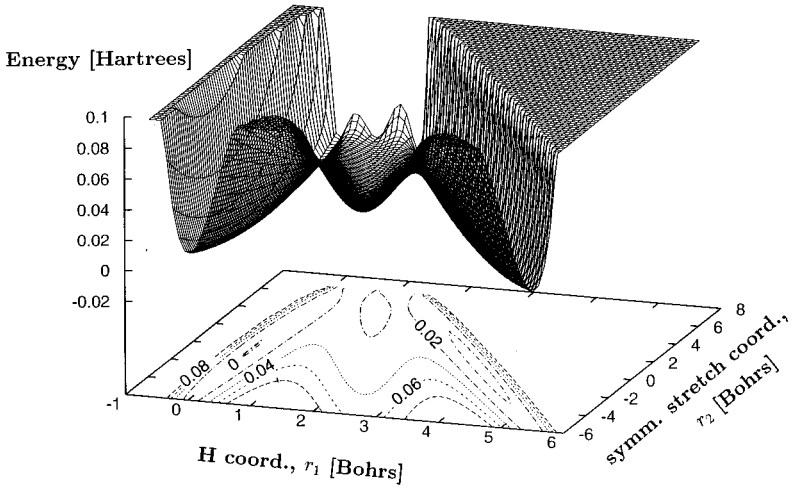

FIG. 5. Zwitterionic reaction surface $V_0^{(z)}(\mathbf{r})$ as a function of r_1 and r_2.

the initial configuration of the dimer is achieved at the intermediate and tautomeric geometries, while the rearrangements for both of the two transition state geometries are quite comparable in magnitude and increase monotonically with the intermonomer separation.

Figure 3 shows the optimized CIS/6-31G energy data points $V_{opt}(r_1(3),r_2)$ for the ''covalent'' intermediate INT.(C), and the corresponding interpolation curve as a function of r_2. This figure shows that the INT.(C) is more stable than the INT.(Z) whenever the intermediate geometry is optimized subject to the constraint of $r_2<4.3$ a.u., and has a global minimum geometry at ($r_2\approx-3.8$ a.u.), which involves a much larger intermonomer separation than in the INT.(Z) minimum energy geometry where the two monomers are much closer together ($r_2\approx4.6$ a.u.).

The covalent reaction surface $V_0^{(c)}$, displayed in Fig. 6, has a minimum equilibrium geometry at about $r_1=2.25$ a.u. and $r_2=-3.8$ a.u.—i.e., significantly displaced relative to the position of the zwitterionic intermediate minimum energy geometry, displayed in Fig. 5 at about $r_1=1.0$ a.u. and $r_2=4.6$ a.u.— and is described according to the quadratic approximation

$$V_0^{(c)}(r_1,r_2)=V_{opt}^{(c)}(r_1(3),r_2)+\frac{1}{2}[\omega_{r_1}^{(c)}(r_2)]^2[r_1(3)-r_1]^2, \tag{2.15}$$

which is a model limited to only configurations within the accessible energy range near the $r_1(3)$ optimized geometries displayed in Fig. 4; $\omega_{r_1}^{(c)}(r_2)$ are the CIS proton frequencies at the $(r_1(3),\ r_2)$ configuration. The covalent potential energy surface $V^{(c)}(r_1,r_2,R)$ is then obtained in terms of the reaction surface $V_0^{(c)}(r_1,r_2)$ according to Eq. (2.13), where the average frequency $\omega_R^{(c)}\approx 350\ \mathrm{cm}^{-1}$.

Figure 9 shows the adiabatic Born–Oppenheimer $S1$ PES for three different values of R that correspond approximately to the F.C. initial geometry ($R=-1.5$ a.u.), the optimized $S1$ base-pair configuration ($R=0$ a.u.), and the tautomeric equilibrium geometry ($R=1.5$ a.u.). The first feature to note when comparing the B.O. PES at the three different configurations of the reorganization coordinate R is that according to our model potential the reactant B.P. is more

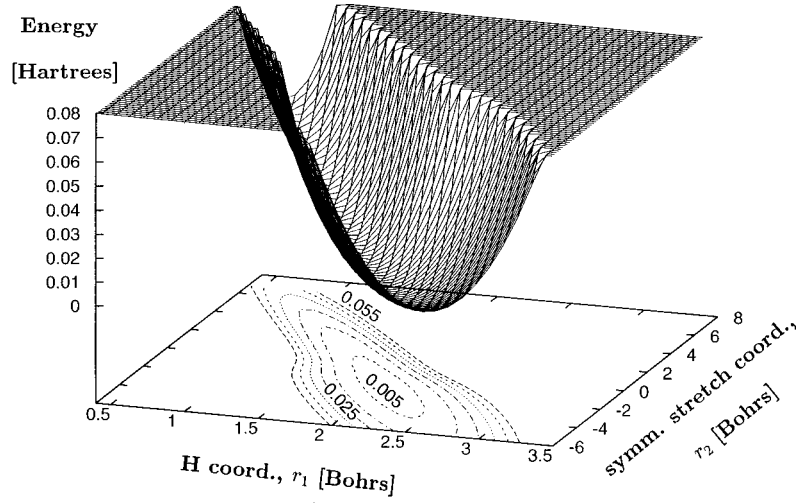

FIG. 6. Covalent reaction surface $V_0^{(c)}(\mathbf{r})$ as a function of r_1 and r_2.

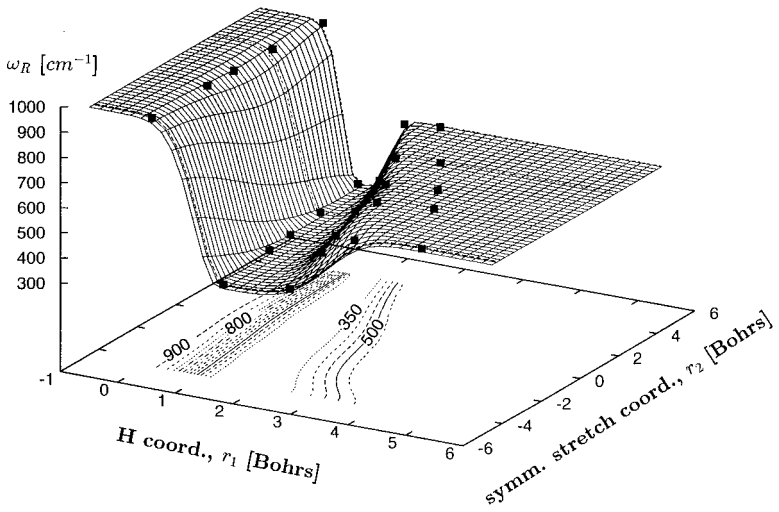

FIG. 7. Harmonic frequency $\omega_R^{(z)}$ of the reorganization coordinate R as a function of r_1 and r_2, and CIS frequency data points (solid squares).

stable than the intermediate or product tautomer in the -1.5–0 a.u. range of R. However, the relative stability changes in favor of the intermediate and product tautomer when R is further increased through reorganization of the dimer. Figure 9 also shows that R modulates the relative stability of the covalent and zwitterionic states, changing significantly the intermediate minimum energy geometry from $\mathbf{r}\approx(1.0,4.6)$ a.u. when $R=-1.5$ a.u., to $\mathbf{r}\approx(2.0,-4.3)$ a.u. when $R=1.5$ a.u. These changes of relative energies in the B.P., INT. and TAU. configurations also affect the energy barrier heights, and the proton transfer thus becomes effectively coupled to both the symmetric stretch coordinate and the motion of the remaining degrees of freedom in the system.

III. RESULTS

We present our results in three subsections. First, in Sec. III A we present the comparison of the semiclassical wave packet motion with the corresponding full quantum mechanical results. In Sec. III B, we then present the analysis of the time dependent reactant population obtained according to our semiclassical methodology, and the comparison with the full quantum mechanical calculations. Finally, in Sec. III C we present the analysis of the isotopic substitution effect.

SC results were converged with 300 000 trajectories integrated according to a standard fourth-order Runge–Kutta algorithm,[84] with a 0.025 fs integration step, using the parallel programming model described in Ref. 91. Parameters $\gamma(j)$ introduced by Eq. (2.4) for each individual coordinate j, were set according to the initial wavefunction dispersion of the corresponding coordinates.[91] All forces and second derivatives necessary for integrating the equations of motion were calculated using finite difference expressions.

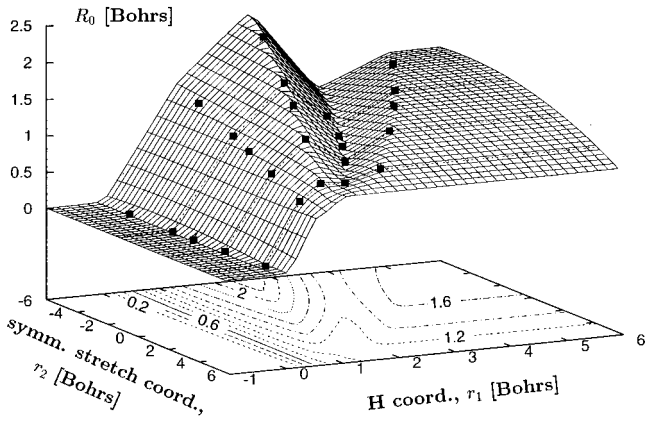

FIG. 8. Equilibrium position R_0 of the reorganization coordinate R as a function of r_1 and r_2, and CIS data points (solid squares).

A. Wave packet motion

Figure 10 compares the evolution of the semiclassical wave packet $\rho(\mathbf{r})=\Psi^*(\mathbf{r})\Psi(\mathbf{r})$ in the space of reaction coordinates $\mathbf{r}$ —i.e., after integrating out the reorganization coordinate R— with the corresponding full quantum mechanical results at various different times during the early time relaxation. Wave packets are represented by five contour lines equally spaced by 0.045 units in the 0.005–0.0185 range of amplitude. The distribution of population among the base-pair, intermediate and tautomer configurations can be visualized in Fig. 10 from the superimposed equilibrium coordinates, introduced by Fig. 4, for the three stationary state proton coordinates $r_1(1)$,$r_1(3)$ and $r_1(5)$ as a function of r_2.

As illustrated by panels (a) and (b), the system is initially localized at the Franck–Condon region with $\mathbf{r}\approx(0.0,-1.33,)$ a.u., and moves during the first 100 fs in the direction of the symmetric-stretch coordinate r_2 approaching the two monomers with respect to each other. During this early time relaxation process the wave packet remains localized in the B.P. region around the r_1 equilibrium positions, but undergoing reorganization of the remaining degrees of freedom in the system. Compared to the quantum mechanical results, our semiclassical wave packets are in excellent agreement. Panel (c) shows the wave packet right after the initial relaxation process at $t=100$ fs, reaching a turning point along the symmetric-stretch coordinate at $\mathbf{r}\approx(0.0,2.3)$ a.u., where the effective barrier heights —from the B.P to the

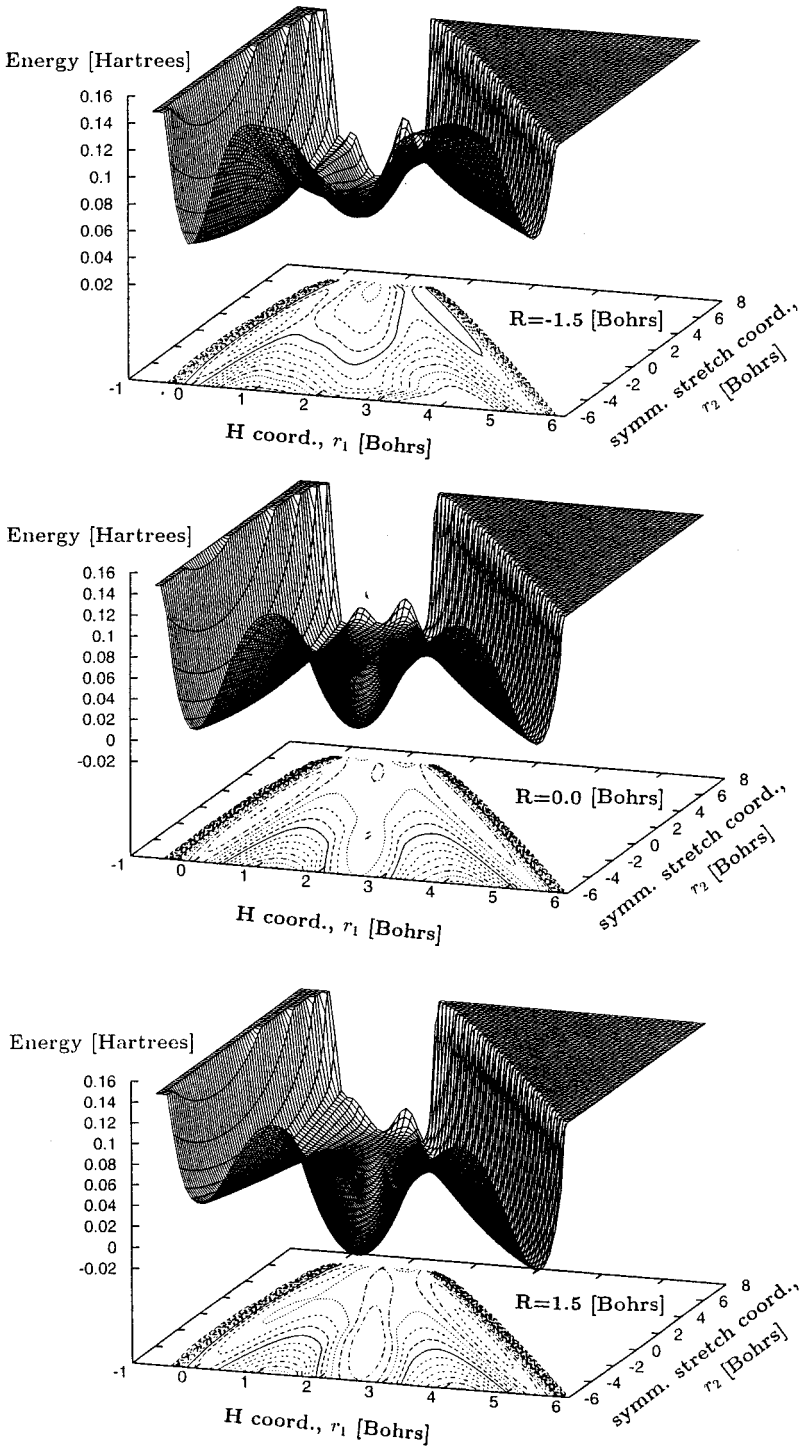

FIG. 9. The Born–Oppenheimer potential energy surface as a function of r_1 and r_2, at three different values of R, including the approximate initial geometry ($R=-1.5$ a.u.), the optimized base pair geometry ($R=0$ a.u.) and the tautomeric configuration ($R=1.5$ a.u.).

INT. configurations— are minimum and the proton transfer is most favorable. Once again, there is very good agreement with the full quantum mechanical results, including the description of both the shape and position of the wave packet, and the proton transfer process in terms of the wave packet spreading into intermediate configurations up to $\mathbf{r}\approx(1.,4.0)$ a.u. Panel (d) shows the wave packet at $t=164$ fs. At this later time, the wave packet in the reactant channel is now displaced towards the F.C. region when compared to its position in panel (c), and there is very good agreement with the quantum mechanical results in terms of its shape and position. Panel (d) also shows that the transmitted population is distributed into intermediate and tautomeric configurations, with intermediate geometries relaxed up to $\mathbf{r}\approx(2.0,0.0)$ a.u., and the tautomer at $\mathbf{r}\approx(2.5,3.5)$ a.u. The comparison with quantum mechanical results is once again very satisfactory. The semiclassical wave packet reproduces the most important features in the full quantum mechanical distribution of populations, and presents only small amplitude deviations displayed by the 0.005 amplitude contour line.

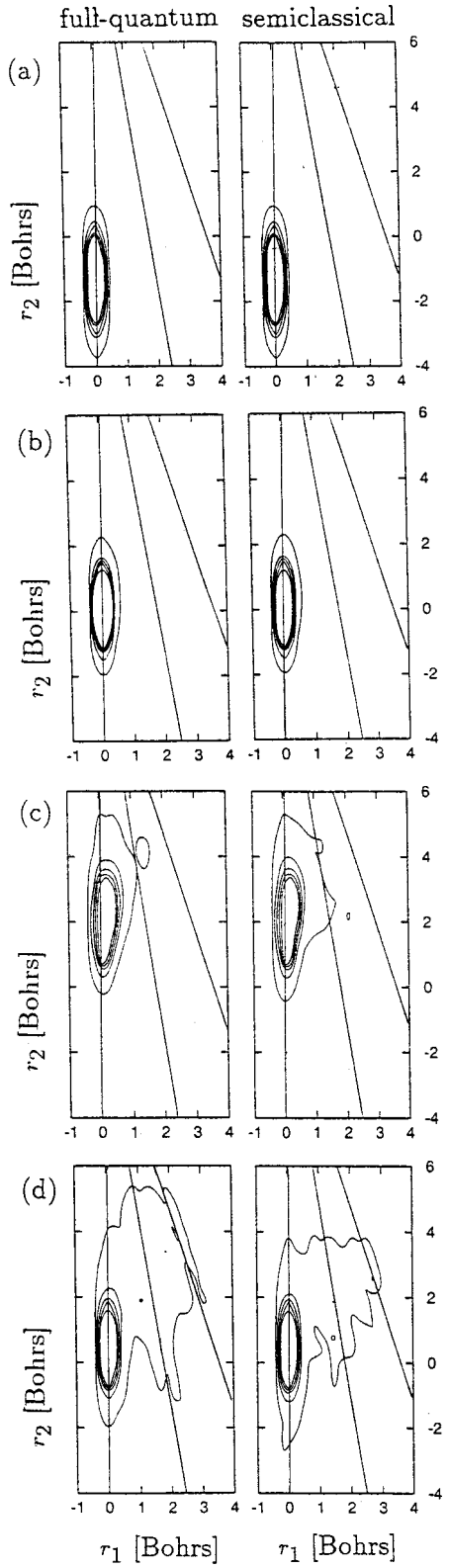

FIG. 10. A comparison between the semiclassical and the full quantum mechanical wave packet $\rho(\mathbf{r})=\Psi^*(\mathbf{r})\Psi(\mathbf{r})$, reduced to the space of reaction coordinates r_1 and r_2 at various different times during the early time relaxation after photo-excitation of the system [Panel (a): 0 fs; panel (b): 48 fs; panel (c): 97 fs; panel (d): 164 fs). Wave packets are represented by five contour lines equally spaced by 0.045 units in the 0.005–0.185 range of amplitude.

B. Reactant population decay

Figure 11 shows the comparison between the semiclassical time dependent reactant population $P(t)$ and the corresponding full quantum mechanical results for the early time tautomerization dynamics where $P(t)$ show the more significant changes, while at longer times $P(t)$ changes only very slowly and SC calculations demand a lot more computational time. As described in Sec. II A, $P(t)$ is obtained according to Eq. (2.1) projecting the time dependent wave packet into the reactant base-pair region according to a dividing surface which defines the transition state position $r_1(2)$ as a function of r_2.

The first feature to note when comparing the semiclassical reactant population decay with full quantum mechanical results is that all the features are well reproduced by our SC calculations, including the initial delay time $\Delta t=$ 60–100 fs, the overall population decay of about 15 percent, and the superimposed modulation with a period of about 40 fs. All of these features can be interpreted in terms of the wave packet motion described in Sec. III A. The initial delay time corresponds to the motion along the symmetric-stretch coordinate (with CIS eigenfrequency $\omega\approx 118$ cm^{-1}), when the two monomers approach each other reducing the effective barrier heights and the probability of proton transfer increases. The superimposed modulation, with a period of about 40 fs, is assigned to the reorganization of the remaining degrees of freedom in the system with $\omega_R\approx$ 900 cm^{-1}. The reduced dimensionality model, however, presents its natural limitations with regards to the proper description of vibrational energy redistribution at longer times. These limitations of the model could, in principle, be overcome by describing all normal mode coordinates explicitly as described in Sec. II C before reducing the dimensionality of the model. This more complete description will be presented in future work.[92]

C. Isotopic effect

Figure 12 shows the comparison between the time dependent reactant population $P(t)$, and the corresponding reactant population decay of the deuterated system. We simulate the relaxation dynamics during the first picosecond after photoexcitation of the system, in terms of the effective potential,[57]

$$V_{eff}=V_{B.O.}+\epsilon, \tag{3.1}$$

where $V_{B.O}$ is the Born–Oppenheimer PES, and the absorbing potential ϵ is defined according to

$$\epsilon(r_1,r_2)=\begin{cases}0, & r_1<r_1(3),\\ -i\gamma[\omega_H]^2[r_1-r_1(3)]^4, & r_1>r_1(3),\end{cases} \tag{3.2}$$

where $\gamma=m_H/(2r_0^2)$, with m_H the proton mass and r_0 the initial proton equilibrium position, while $\omega_H=3500$ cm^{-1}, and $r_1(3)$ represents the position of the intermediate configuration as a function of r_2. This effective potential simulates approximately dynamics in reduced dimensionality assuming that the excess energy in the reaction coordinates is efficiently absorbed by the remaining degrees of freedom once the system evolves beyond the intermediate configura-

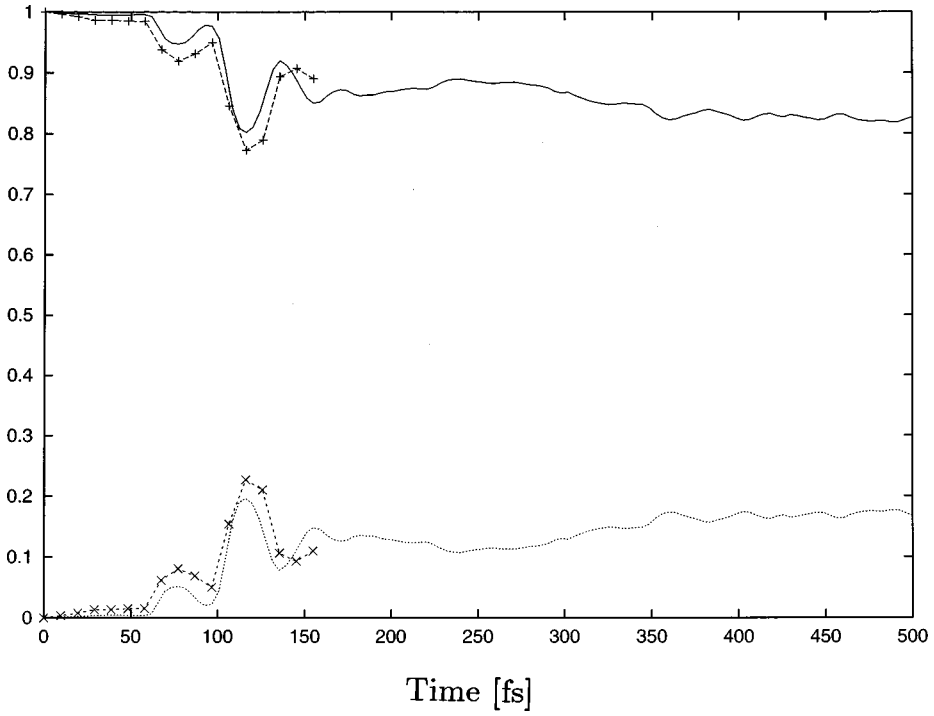

FIG. 11. A comparison between the semiclassical time dependent reactant population $P(t)$ (plus symbols), and the corresponding full quantum mechanical results (solid line) for the early time tautomerization dynamics. The total probability of proton transfer is represented in crosses (semiclassical) and dots (quantum mechanical).

tions. Figure 12 shows that the time dependent reactant population drops at time intervals of $\sim$200 fs after an initial 100 fs delay time, and also that the isotopic substitution reduces significantly the transmitted amount —i.e., the proton transfer probability— but does not affect the time intervals at which we observe population decay. These observations can be well understood in terms of the description of the wave packet motion presented in Sec. III A: the initial relaxation process does not involve any significant proton displacement, and the system moves only along the symmetric-stretch coordinate with some reorganization of the remaining degrees of freedom. The transmitted amount, however, is significantly reduced when H is substituted by D with a lower zero point energy and a more localized wave function.

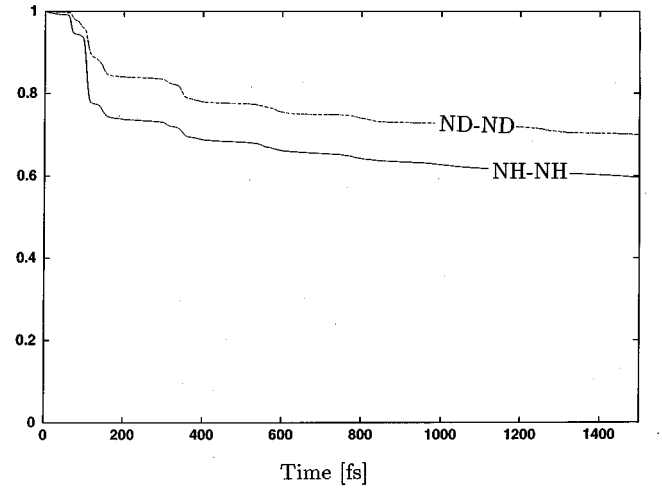

FIG. 12. A comparison between the time dependent reactant population (solid line), and the corresponding reactant population decay of the deuterated system (long dashes).

Comparing the early time relaxation dynamics presented in Fig. 12 for the undeuterated species with the population decay displayed earlier in Fig. 11, we see that the most important effect of the absorbing potential is to eliminate the recrossing dynamics which is modulated by the reorganization coordinate R. The agreement displayed in Fig. 11 between the SC and the full quantum mechanical description of the superimposed structure indicates that the approximate SC-IVR method provides a proper description of dynamics, even in the presence of recrossing and tunneling.

IV. CONCLUSIONS AND COMPARISONS WITH EXPERIMENTS

We have shown in this paper how the ultrafast excited state double-proton transfer dynamics involved in the tautomerization reaction of the photo-excited 7-azaindole dimers can be investigated in terms of an approximate semiclassical initial value representation method to model quantum reaction dynamics. The main idea in the approximate semiclassical approach is to integrate the dynamical variables necessary for the calculation of the classical probability associated with individual trajectories —i.e., the pre-exponential factor $C_t(\mathbf{p_0},\mathbf{q_0})$— according to the adiabatic approximation, reducing the computational effort to the propagation of only $O(N)$ independent dynamical variables after diagonalization of the Hessian.

We have demonstrated the capabilities of the approximate semiclassical method to study the excited state double-proton transfer dynamics in 7-azaindole dimers, showing good agreement with full quantum mechanical calculations in describing all dynamical features in the wave packet motion and the reactant population decay, even in the presence of tunneling and recrossing events. The approximate semiclassical approach aims to provide a more tractable alterna-

tive to exact quantum mechanical methods for dynamics calculations of polyatomic systems in terms of a dynamically consistent treatment of all degrees of freedom, integrated according to fully deterministic classical equations of motion, where quantum effects such as tunneling and interference are included correctly and naturally in the description.

We have shown that the reaction mechanism suggested by our simulation results differs from both of the two reaction mechanisms postulated by recent ultrafast spectroscopic studies, particularly with regards to the nature of the electronic states and the assignment of the characteristic times involved.[31–35,37] In order to make a comparison with these other postulated mechanisms, we first outline the experimental findings and then make contact with our SC MD simulation results. Zewail and co-workers reported studies of the femtosecond dynamics of the isolated pair in a molecular beam using pump-probe time-resolved mass spectroscopy, where the observed biexponential decay was interpreted in terms of a postulated sequential step-wise mechanism.[31,35] The ultrafast component of the biexponential decay was assigned to proton tunneling from an initial base pair to a zwitterionic intermediate, through an estimated energy barrier of about 1.2 kcal/mol, and the fast component was assigned to the tunneling event of the second proton from the zwitterionic state to the tautomer configuration. More recently, their work was extended to investigate the effect of the solution phase on the DPTR in the same pair, using fluorescence upconversion techniques, finding that the fast and ultrafast relaxation constants were similar to those obtained for the isolated base pair.[32,33] Castleman and co-workers reported experiments using Coulomb explosion techniques, which were interpreted in terms of a zwitterionic arrested intermediate.[37] Takeuchi and Tahara,[32,33] reported extensive studies of the DPTR in 7-azaindole dimers in the condensed phase, where they also found biexponential relaxation with similar time constants to those obtained by Zewail and coworkers, but interpreted their results according to a reaction mechanism that involves initial population of the ''^1L_b'' state—assumed to have a larger oscillator strength, and be located at a higher energy than the ''^1L_a'' state—followed by ultrafast electronic relaxation to the ''^1L_a'' state (with a rate constant of 200 fs), and then fast concerted double-proton transfer to the tautomeric form in the same ''^1L_a'' electronic state. These authors ruled out the possibility of assigning the fast fluorescence component to a hypothetical zwitterionic state, since the fluorescence peak at 350 nm was away from the 420–450 nm range expected for the zwitterionic fluorescence. Furthermore, they considered that the ultrafast component was not relevant to the actual proton translocation, since the time constant of the ultrafast component remained unchanged by deuterium substitution.

In this paper we have shown that the adiabatic DPTR in the isolated pair involves a sequential two-step proton translocation process, where for most nuclear configurations the intermediate electronic state is different from the electronic state that was initially populated by photoexcitation of the system. Contrary to having zwitterionic character, the $S1$ intermediate has a ''covalent'' electronic structure for most of the energetically accessible nuclear configurations, since the positive charge associated with the first proton transfer is neutralized by the single intermonomer $(62)\rightarrow(64)$ MO excitation. Our reaction mechanism, however, does not rule out the possibility of detecting transient population on the zwitterionic intermediate state, when proton transfer takes place at fairly small intermonomer separations.

We have shown that the first proton transfer takes place only after the system undergoes nuclear relaxation, a process that approaches the two monomers to configurations where proton transfer is most favorable. The initial nuclear relaxation process involves primarily intermonomer symmetric-stretch motion with a period of about 200 fs which is insensitive to isotopic substitution, together with reorganization of the remaining degrees of freedom in the system, including intermonomer asymmetric stretch motion, and reorganization of single to double aromatic bonds with frequencies characteristic of the C–C and C–N stretching modes. The relaxation process involves an initial 15 percent reactant population decay, with a delay time of about 100 fs after photoexcitation of the system, and further leakage of reactant population at intervals of about 200 fs. Isotopic substitution reduces significantly the amount of transmitted population, but does not affect the timing for the successive events of reactant population depletion.

Finally, we have shown that the populated state with larger oscillator strength constant in the FC region corresponds to the $S1$ state, which although somewhat affected by dimerization is similar to the $S1$ state of the monomer that undergoes preferential geometry reorganization, and thus analogous to the ''^1L_a'' state of condensed ring molecules with predominant (HOMO) $\rightarrow$ (LUMO) MO single excitation. We have also shown that the state analogous to the ''^1L_b'' state of condensed ring molecules—i.e., with predominant (HOMO) $\rightarrow$ (LUMO+1) MO single excitation—corresponds to the $S2$ state and has a smaller transition dipole moment.

In this paper we have not presented a comparison between our population decay profiles and the experimental signals, since simply raising the ground state population up to the excited state corresponds to irradiating with a broad band of frequencies which populate only the $S1$ electronic state. Our interest here was thus to characterize the electronic state with larger oscillator strength constant and simulate the relaxation dynamics made available by nuclear and electronic processes, sampling all the possible types of initial conditions at the low-temperature limit. However, the more ambitious task of simulating specific time dependent experimental signals is the subject of future work,[92] where the approximate SC-IVR method is implemented according to a reaction surface model potential in higher dimensionality.

ACKNOWLEDGMENTS

We gratefully acknowledge financial support from the Director, Office of Science, Office of Basic Energy Sciences, Chemical Sciences Division of the U.S. Department of Energy under Contract No. DE-AC03-76SF00098, by the Laboratory Directed Research and Development (LDRD) project from the National Energy Research Scientific Computing Center (NERSC), Lawrence Berkeley National Laboratory,

and by the National Science Foundation under Grant No. CHE-9732758. We also acknowledge a generous allocation of supercomputing time from the National Energy Research Scientific Computing Center (NERSC).

APPENDIX: APPROXIMATE SC-IVR METHOD

Here we present the derivation of the approximate pre-exponential factor $C_t(\mathbf{p_0},\mathbf{q_0})$ given by Eqs. (2.7)–(2.9) and used for all the SC calculations in this paper. The exact expression for the HK pre-exponential factor is

$$C_t(\mathbf{p}_0,\mathbf{q}_0)=\sqrt{\det[\mathbf{M}_t]}, \tag{A1}$$

where the matrix $\mathbf{M}_t$ is the following linear combination of components of the monodromy matrix:

$$\mathbf{M}_t=\frac{1}{2}\left[\frac{\partial \mathbf{q}_t}{\partial \mathbf{q}_0}+\boldsymbol{\gamma}^{-1}\cdot\frac{\partial \mathbf{p}_t}{\partial \mathbf{p}_0}\cdot\boldsymbol{\gamma}-\frac{1}{2i\hbar}\boldsymbol{\gamma}^{-1}\frac{\partial \mathbf{p}_t}{\partial \mathbf{q}_0}-2i\hbar\frac{\partial \mathbf{q}_t}{\partial \mathbf{p}_0}\cdot\boldsymbol{\gamma}\right], \tag{A2}$$

where $\boldsymbol{\gamma}$ is the diagonal matrix whose elements are the coherent state parameters in Eq. (2.4), and

$$\left(\frac{\partial \mathbf{q}_t}{\partial \mathbf{q}_0}\right)_{i,j}=\frac{\partial \mathbf{q}_t(i)}{\partial \mathbf{q}_0(j)},\ \text{etc.} \tag{A3}$$

Defining the matrices $\mathbf{Q}_t$ and $\mathbf{P}_t$ as the following linear combinations of the monodromy matrix elements:

$$\begin{aligned}\mathbf{Q}_t&=\frac{\partial \mathbf{q}_t}{\partial \mathbf{q}_0}-2i\hbar\left(\frac{\partial \mathbf{q}_t}{\partial \mathbf{p}_0}\right)\cdot\boldsymbol{\gamma},\\ \mathbf{P}_t&=\frac{\partial \mathbf{p}_t}{\partial \mathbf{q}_0}-2i\hbar\left(\frac{\partial p_t}{\partial p_0}\right)\cdot\boldsymbol{\gamma},\end{aligned} \tag{A4}$$

one sees that the matrix $\mathbf{M}_t$ of Eq. (A2) is given by

$$\mathbf{M}_t=\frac{1}{2}\left(\mathbf{Q}_t+\frac{i}{2\hbar}\boldsymbol{\gamma}^{-1}\cdot\mathbf{P}_t\right). \tag{A5}$$

Furthermore, the matrices $\mathbf{Q}_t$ and $\mathbf{P}_t$ can be obtained by integrating the following equations:

$$\begin{aligned}\dot{\mathbf{Q}}_t&=\mathbf{P}_t,\\ \dot{\mathbf{P}}_t&=-\mathbf{K}_t\cdot\mathbf{Q}_t,\end{aligned} \tag{A6}$$

where $\mathbf{K}_t$ is the Hessian (or mass-weighted force constant) matrix at time t along the trajectory,

$$(\mathbf{K}_t)_{i,j}=\frac{\partial^2 V_{B.O.}(\mathbf{q_t})}{\partial q_t(i)\partial q_t(j)}; \tag{A7}$$

the initial conditions for Eq. (A6) are

$$\begin{aligned}\mathbf{Q}_0&=\mathbf{1},\\ \mathbf{P}_0&=-2i\hbar\boldsymbol{\gamma}.\end{aligned} \tag{A8}$$

The exact calculation of the matrix $\mathbf{M}_t$ (and thus the pre-exponential factor, as its determinant) thus requires one to integrate the matrix equations (A6), with initial conditions (A8), with $\mathbf{M}_t$ then being given by Eq. (A5). The integration of these equations is an $O(N^2)$ process because of the matrix operations that are involved.

The adiabatic approximation is suggested by noting that the two equations (A6) can be combined to read

$$\ddot{\mathbf{Q}}_t=-\mathbf{K}_t\cdot\mathbf{Q}_t, \tag{A9}$$

which is isomorphic to an N-state coupled channel Schrödinger equation (with t playing the role of the ''translational coordinate''). The adiabatic approximation to this is obtained by introducing the orthogonal transformation $\mathbf{L}_t$ that diagonalizes the Hessian $\mathbf{K}_t$ at each time t,

$$\mathbf{L}_t^{\dagger}\cdot\mathbf{K}_t\cdot\mathbf{L}_t\equiv\boldsymbol{\omega}_t^2, \tag{A10}$$

where $\boldsymbol{\omega}_t$ is a diagonal matrix of frequencies (c.f. the ''instantaneous normal modes''). If one neglects time derivatives of $\mathbf{L}_t$—this is the adiabatic approximation— then the transformed matrices $\tilde{\mathbf{Q}}_t$ and $\tilde{\mathbf{P}}_t$,

$$\begin{aligned}\tilde{\mathbf{Q}}_t&\equiv\mathbf{L}_t^{\dagger}\cdot\mathbf{Q}_t\cdot\mathbf{L}_t,\\ \tilde{\mathbf{P}}_t&\equiv\mathbf{L}_t^{\dagger}\cdot\mathbf{P}_t\cdot\mathbf{L}_t,\end{aligned} \tag{A11}$$

remain diagonal at all times t. The diagonal elements are obtained by integrating the N one-dimensional equations,

$$\begin{aligned}\dot{\tilde{Q}}_t(k,k)&=\tilde{P}_t(k,k),\\ \dot{\tilde{P}}_t(k,k)&=-\omega_t(k)^2\tilde{Q}_t(k,k),\end{aligned} \tag{A12}$$

for $k=1,\ldots,N$, with initial conditions

$$\begin{aligned}\tilde{Q}_0(k,k)&=1,\\ \tilde{P}_0(k,k)&=-2i\hbar\gamma(k).\end{aligned} \tag{A13}$$

Finally, the matrix $\mathbf{M}_t$ is then given by

$$\mathbf{M}_t=\mathbf{L}_t\cdot\frac{1}{2}\left(\tilde{\mathbf{Q}}_t+\frac{i}{2\hbar}\gamma^{-1}\cdot\tilde{\mathbf{P}}_t\right)\cdot\mathbf{L}_t^{\dagger}, \tag{A14}$$

and since $\det(\mathbf{L}_t)=\det(\mathbf{L}_t^{\dagger})=1$, one has

$$\begin{aligned}\det(\mathbf{M}_t)&=\det\left[\frac{1}{2}\left(\tilde{\mathbf{Q}}_t+\frac{i}{2\hbar}\boldsymbol{\gamma}^{-1}\cdot\tilde{\mathbf{P}}_t\right)\right],\\ &=\prod_{k=1}^{N}\frac{1}{2}\left(\tilde{Q}_t(k,k)+\frac{i}{2\hbar}\gamma(k)^{-1}\tilde{P}_t(k,k)\right),\end{aligned} \tag{A15}$$

whereby Eq. (A1) gives the adiabatic pre-exponential factor described in Sec. II A.

This adiabatic approximation should be good if the frequencies $\omega_t(k)$ remain well separated (or the local normal modes are not strongly coupled) along the trajectory, but we note that the pre-exponential factor will also be given correctly by this approximation in the *opposite* limit, i.e., if the frequencies undergo a sharply avoided crossing (local Fermi resonance) at some time t. In this ''diabatic'' limit the instantaneous frequencies ($\equiv$ the potential energy curves in the analogy to coupled-channel Schrödinger equation) simply re-label themselves, and since the pre-exponential factor involves the *determinant*, i.e., a product of them all, the order of the product is immaterial. One thus has the fortuitous situation that the result for C_t will be given correctly, not only in the adiabatic limit but also in the diabatic limit. One can hope that it will not be too far off in intermediate cases.

Finally, we note that it may sometimes be useful to solve the one-dimensional equations (A12) with a WKB approximation. With the boundary conditions of Eq. (A13) this gives

$$\begin{aligned}\tilde{Q}_t(k,k) &= \left(\frac{\omega_0(k)}{\omega_t(k)}\right)^{1/2}\cos\left(\int_0^t dt'\,\omega_{t'}(k)\right) \\ &\quad - \frac{2i\hbar\gamma(k)}{(\omega_0(k)\omega_t(k))^{1/2}}\sin\left(\int_0^t dt'\,\omega_{t'}(k)\right), \\ \tilde{P}_t(k,k) &= -(\omega_0(k)\omega_t(k))^{1/2}\sin\left(\int_0^t dt'\,\omega_{t'}(k)\right) \\ &\quad - 2i\hbar\gamma(k)\left(\frac{\omega_t(k)}{\omega_0(k)}\right)^{1/2}\cos\left(\int_0^t dt'\,\omega_{t'}(k)\right).\end{aligned} \tag{A16}$$

so that Eq. (A15) becomes

$$\begin{aligned}\det(\mathbf{M}_t) &= \prod_{k=1}^{N}\frac{1}{2}\left(\sqrt{\frac{\omega_0(k)}{\omega_t(k)}}+\sqrt{\frac{\omega_t(k)}{\omega_0(k)}}\right) \\ &\quad\times\cos\left(\int_0^t dt'\,\omega_{t'}(k)\right) - \frac{i}{2}\left(\frac{2\hbar\gamma(k)}{\sqrt{\omega_0(k)\omega_t(k)}}\right. \\ &\quad\left.+\frac{\sqrt{\omega_0(k)\omega_t(k)}}{2\hbar\gamma(k)}\right)\sin\left(\int_0^t dt'\,\omega_{t'}(k)\right).\end{aligned} \tag{A17}$$

This WKB approximation, however, does not take account of reflections that occur at classical turning points or avoided crossings, and is thus probably a much cruder approximation than integrating the one-dimensional equations (A12) exactly.

[1] V. A. Benderskii, D. E. Makarov, and C. A. Wight, Adv. Chem. Phys. **88**, 1 (1994).
[2] Y. Cha, C. J. Murray, and J. P. Klinman, Science **243**, 1325 (1989).
[3] M. E. Tuckerman, D. Marx, M. L. Klein, and M. Parrinello, Science **275**, 817 (1997).
[4] A. Luzar and D. Chandler, Nature (London) **379**, 55 (1996).
[5] J. K. Gregory and D. C. Clary, J. Chem. Phys. **105**, 6626 (1996).
[6] A. Warshel, A. Papazyan, and P. A. Kollman, Science **269**, 102 (1995).
[7] T. Bountis, in *Proton Transfer in Hydrogen-Bonded Systems* (Plenum, New York, (1992).
[8] W. W. Cleland and M.M. Kreevoy, Science **264**, 1887 (1994).
[9] P. A. Frey, S. A. Whitt, and J. B. Tobin, Science **264**, 1927 (1994).
[10] D. F. Brougham, A. J. Horsewill, and R. I. Jenkinson, Chem. Phys. Lett. **272**, 69 (1997).
[11] L. B. Clark, G. G. Peschel, and I. Tinoco, Jr., J. Phys. Chem. **69**, 3615 (1965).
[12] M. Fujii, T. Tamura, N. Mikami, and M. Ito, Chem. Phys. Lett. **126**, 583 (1986).
[13] C. A. Taylor, M. A. El-Bayoumi, and M. Kasha, Proc. Natl. Acad. Sci. USA **63**, 253 (1969).
[14] M. A. El-Bayoumi, P. Avouris, and W. R. Ware, J. Chem. Phys. **62**, 2499 (1975).
[15] K. C. Ingham, M. Abu-Elgheit, and M. A. El-Bayoumi, J. Chem. Phys. **93**, 5023 (1971).
[16] K. C. Ingham and M. A. El-Bayoumi, J. Am. Chem. Soc. **96**, 1 (1974).
[17] K. Fuke, H. Yoschiuchi, and K. Kaya, J. Phys. Chem. **88**, 5840 (1984).
[18] K. Fuke and K. Kaya, J. Phys. Chem. **93**, 614 (1989).
[19] Waluk J. Habilitation Thesis, Warsawa University, 1986.
[20] S. J. Formosinho and J. Arnaut, J. Photochem. Photobiol., A **75**, 21 (1993).
[21] A. Douhal, V. Guallar, M. Moreno, and J. M. Lluch, Chem. Phys. Lett. **256**, 370 (1996).
[22] J. Waluk, A. Grabowska, and J. Lipinski, Chem. Phys. Lett. **70**, 175 (1980).
[23] V. I. Pechenaya and V. I. Danilov, Chem. Phys. Lett. **11**, 539 (1971).
[24] J. Catalan and P. Perez, J. Theor. Biol. **81**, 213 (1979).
[25] J. Waluk, H. Bulska, A. Grabowska, and A. N. Mordzinski, New J. Chem. **10**, 413 (1986).
[26] H. Bulska, A. Grabowska, B. Paluka, J. Sepiol, and J. Waluk, J. Lumin. **29**, 65 (1984).
[27] J. A. Herek, S. Pedersen, L. Banares, and A. H. Zewail, J. Chem. Phys. **97**, 9046 (1992).
[28] V. K. Babamov and R. A. Marcus, J. Chem. Phys. **74**, 1790 (1981).
[29] W. M. Hetherington, III, R. H. Micheels, and K. B. Eisenthal, Chem. Phys. Lett. **66**, 230 (1979).
[30] P. Share, M. Pereira, M. Sarisky, S. Repinec, and R. M. Hochstrasser, J. Lumin. **48**, 204–208 (1991).
[31] A. Douhal, S. K. Kim, and A. H. Zewail, Nature (London) **378**, 260 (1995).
[32] S. Takeuchi and T. Tahara, Chem. Phys. Lett. **277**, 340 (1997).
[33] S. Takeuchi and T. Tahara, J. Phys. Chem. **102**, 7740 (1998).
[34] R. Lopez Martens, P. Long, D. Solgadi, B. Soep, J. Syage, and Ph. Millie, Chem. Phys. Lett. **273**, 219 (1997).
[35] M. Chachisvilis, T. Fiebig, A. Douhal, and A. H. Zewail, J. Phys. Chem. **102**, 669 (1998).
[36] A. Douhal, F. Lahmani, and A. H. Zewail, Chem. Phys. **207**, 477 (1996).
[37] D. E. Folmer, L. Poth, E. S. Wisniewski, and A. W. Casteleman, Chem. Phys. **291**, 101 (1997).
[38] J. D. H. Watson and F. H. C. Crick, Nature (London) **171**, 737 (1953).
[39] P. O. Lowdin, Adv. Quantum Chem. **2**, 213 (1965).
[40] M. F. Goodman, Nature (London) **378**, 237 (1995).
[41] J. M. Lehn, in *Supramolecular Chemistry: Concepts and Perspectives* (VCH, New York, 1995).
[42] N. Makri and W. H. Miller, J. Chem. Phys. **91**, 4026 (1989).
[43] T. Carrington, Jr. and W. H. Miller, J. Chem. Phys. **84**, 4364 (1986).
[44] S. Hammes-Schiffer and J. C. Tully, J. Chem. Phys. **101**, 4657 (1994).
[45] J. Y. Fang and S. Hammes-Schiffer, J. Chem. Phys. **107**, 8933 (1997).
[46] W. H. Miller, J. Chem. Phys. **62**, 1899 (1975).
[47] V. A. Benderskii, V. I. Goldanskii, and D. E. Makarov, Phys. Rep. **233**, 195 (1993).
[48] F. Grossmann and E. J. Heller, Chem. Phys. Lett. **241**, 45 (1995).
[49] M. F. Herman and E. Kluk, Chem. Phys. **91**, 27 (1984).
[50] K. G. Kay, J. Chem. Phys. **107**, 2313 (1997).
[51] H. Ushiyama and K. Takatsuka, J. Chem. Phys. **106**, 7023 (1997).
[52] B. C. Garrett and D. G. Truhlar, J. Chem. Phys. **79**, 4931 (1983).
[53] A. Warshel and Z. T. Chu, J. Chem. Phys. **93**, 4003 (1990).
[54] J. Cao and G. A. Voth, J. Chem. Phys. **101**, 6168 (1994).
[55] D. Borgis and J. T. Hynes, J. Chem. Phys. **94**, 3619 (1991).
[56] S. Keshavamurthy and W. H. Miller, Chem. Phys. Lett. **218**, 189 (1994).
[57] B. Spath and W. H. Miller, J. Chem. Phys. **104**, 95 (1996).
[58] N. Sato and S. Iwata, J. Chem. Phys. **89**, 2932 (1988).
[59] R. A. Marcus, J. Chem. Phys. **45**, 4493 (1966).
[60] W. H. Miller, N. C. Handy, and J. E. Adams, J. Chem. Phys. **72**, 788 (1980).
[61] K. Fukui, Acc. Chem. Res. **14**, 363 (1981).
[62] S. A. Adelman and J. D. Doll, J. Chem. Phys. **61**, 4242 (1974).
[63] M. Shuggard, J. C. Tully, and A. Nitzan, J. Chem. Phys. **66**, 2534 (1977).
[64] G. C. Schatz, Chem. Phys. **31**, 295 (1978).
[65] R. A. Marcus, J. Chem. Phys. **46**, 959 (1967).
[66] T. Carrington, Jr. and W. H. Miller, J. Chem. Phys. **81**, 3942 (1984).
[67] J. C. D. Brand and Ch. V. S. Ramachandra Rao, J. Mol. Spectrosc. **61**, 360 (1976).
[68] P. Russegger, Chem. Phys. **41**, 299 (1979).
[69] P. Russegger, Chem. Phys. Lett. **69**, 362 (1980).
[70] V. Szalay, J. Mol. Spectrosc. **102**, 13 (1983).
[71] J. M. Bowman, G. Z. Ju, and K. T. Lee, J. Chem. Phys. **75**, 5199 (1981).
[72] M. Morillo and R. I. Cukier, J. Chem. Phys. **92**, 4833 (1990).
[73] A. Suarez and R. Silbey, J. Chem. Phys. **94**, 4809 (1991).
[74] J. Aqvist and A. Warshel, Chem. Rev. **93**, 2523 (1993).
[75] D. G Truhlar, Y. P. Liu, G.K. Schenter, and B. C. Garrett, J. Phys. Chem. **98**, 8396 (1994).
[76] D. Borgis, G. Tarjus, and H. Azzuoz, J. Phys. Chem. **96**, 3188 (1992).
[77] D. Borgis, G. Tarjus, and H. Azzuoz, J. Phys. Chem. **97**, 1390 (1992).
[78] D. Laria, G. Ciccoti, M. Ferrario, and R. Kapral, J. Chem. Phys. **97**, 378 (1992).
[79] A. Fedorowicz, J. Mavri, P. Bala, and A. Koll, Chem. Phys. Lett. **289**, 457 (1998).
[80] M. T. M. Koper and G. A. Voth, Chem. Phys. Lett. **282**, 100 (1998).

[81] Y. G. Boroda, A. Calhoun, and G. A. Voth, J. Chem. Phys. **107**, 8940 (1997).
[82] Yin Guo, A. K. Wilson, C. F. Chabalowski, and D. L. Thompson, J. Chem. Phys. **109**, 9258 (1998).
[83] Y. Guo, S. Li, and D. L. Thompson, J. Chem. Phys. **107**, 2853 (1997).
[84] W. H. Press, B. P. Flannery, S. A. Teukolsky, and W. T. Vetterling, in *Numerical Recipes* (Cambridge University Press, Cambridge, 1986).
[85] M. K. Shukla and P. C. Mishra, Chem. Phys. **230**, 187 (1998).
[86] P. R. Callis, J. Chem. Phys. **95**, 4230 (1991).
[87] A. Warshel, J. Phys. Chem. **86**, 2218 (1982).
[88] X. Sun and W. H. Miller, J. Chem. Phys. **106**, 6346 (1997).
[89] M. J. Frisch, *et al.*, GAUSSIAN94 (Gaussian Inc., Pittsburgh, PA 1995).
[90] D. Kincaid and W. Cheney, in *Numerical Analysis* (Brooks/Cole, Malabar, FL, 1996), p. 335.
[91] V. S. Batista and W. H. Miller, J. Chem. Phys. **108**, 498 (1998).
[92] V. Guallar, V. S. Batista, M. Moreno, J. M. Lluch, and W. H. Miller (in preparation).